Single-domain perpendicular magnetization induced by the coherent O math xmlns="http://www.w3.org/1998/Math/MathML">mrow>mn>2/mn>mi>p/mi>/mrow>/math>-Ru math xmlns="http://www.w3.org/1998/Math/MathML">mrow>mn>4/mn>mi>d/mi>/mrow>/math> hybridized state in an ultra-high-quality math xmlns="http://www.w3.org/1998/Math/MathML">mrow>mi>SrRu/mi>msub>mi mathvariant="normal">O/mi> mn>3/mn>/msub>/mrow>/math> film

Yuki K. Wakabayashi, Masaki Kobayashi, Yukiharu Takeda, Kosuke Takiguchi, Hiroshi Irie, Shin-ichi Fujimori, Takahito Takeda, Ryo Okano, Yoshiharu Krockenberger, Yoshitaka Taniyasu, and Hideki Yamamoto

Phys. Rev. Materials **5**, 124403 — Published 2 December 2021

DOI: 10.1103/PhysRevMaterials.5.124403

Single-domain perpendicular magnetization induced by the coherent O 2*p*-Ru 4*d* hybridized state in an ultra-high-quality $SrRuO_3$ film

Yuki K. Wakabayashi,[1,*,†] Masaki Kobayashi,[2,3,*,‡] Yukiharu Takeda,[4] Kosuke Takiguchi,[1] Hiroshi Irie,[1] Shin-ichi Fujimori,[4] Takahito Takeda,[3] Ryo Okano,[3] Yoshiharu Krockenberger,[1] Yoshitaka Taniyasu,[1] and Hideki Yamamoto[1]

[1]*NTT Basic Research Laboratories, NTT Corporation, Atsugi, Kanagawa 243-0198, Japan*

[2]*Center for Spintronics Research Network, The University of Tokyo, 7-3-1 Hongo, Bunkyo-ku, Tokyo 113-8656, Japan*

[3]*Department of Electrical Engineering and Information Systems, The University of Tokyo, Bunkyo, Tokyo 113-8656, Japan*

[4]*Materials Sciences Research Center, Japan Atomic Energy Agency, Sayo-gun, Hyogo 679-5148, Japan*

[*]These authors contributed equally to this work.

[†]Corresponding author: yuuki.wakabayashi.we@hco.ntt.co.jp

[‡]Corresponding author: masaki.kobayashi@ee.t.u-tokyo.ac.jp

Abstract

We investigated the Ru 4*d* and O 2*p* electronic structure and magnetic properties of an ultra-high-quality $SrRuO_3$ film on $SrTiO_3$ grown by machine-learning-assisted molecular beam epitaxy. The high itinerancy and long quantum lifetimes of the quasiparticles in the Ru 4*d* t_{2g}-O 2*p* hybridized valence band are confirmed by observing the prominent well-screened peak in the Ru 3*d* core-level photoemission spectrum, the coherent peak near the Fermi energy in the valence band spectrum, and quantum oscillations in the resistivity. The element-specific magnetic properties and the hybridization between the Ru 4*d* and O 2*p* orbitals were characterized by Ru $M_{2,3}$-edge and O *K*-edge soft X-ray absorption spectroscopy and X-ray magnetic circular dichroism measurements. The ultra-high-quality $SrRuO_3$ film with the residual resistivity ratio of 86 shows the large orbital magnetic moment of oxygen ions induced by the strong orbital hybridization of the O 2*p* states with the spin-polarized Ru 4*d* t_{2g} states. The film also shows single-domain perpendicular magnetization with an almost ideal remanent magnetization ratio of 0.97. These results provide detailed insights into the relevance between orbital hybridization and the perpendicular magnetic anisotropy in $SrRuO_3/SrTiO_3$ systems.

I. INTRODUCTION

The itinerant 4*d* ferromagnetic perovskite $SrRuO_3$ [bulk Curie temperature (T_C) = 160 K] has been studied extensively for many decades because of the unique nature of its ferromagnetism, metallicity, chemical stability, and compatibility with other perovskite-structured oxides [1–21]. Unlike many perovskite transition-metal oxides, the spin-polarized Ru 4*d* orbitals hybridized with the O 2*p* orbitals in $SrRuO_3$ have the itinerant character despite the strong electron correlation [8]. Therefore, $SrRuO_3$ is widely used as a ferromagnetic metal electrode in oxide electronic and spintronic devices consisting of perovskite layers. In addition, the perpendicular magnetic anisotropy induced by the compressive strain [7,8,20] is beneficial for scalability and the reduction of power consumption in spintronic devices, such as magnetic random access memory, and thus $SrRuO_3$-based all-oxide spintronic devices have been investigated [15,16,22].

$SrRuO_3/SrTiO_3$ is the first oxide heterostructure in which perpendicular magnetic anisotropy was discovered [23], and it has been a model system for understanding it in metallic oxides [24,25]. It has been generally considered that perpendicular magnetic anisotropy arises from magnetocrystalline anisotropy caused by spin-orbit interactions. Bruno has demonstrated that the magnetocrystalline anisotropy energy is proportional to the difference in the orbital magnetic moment between the perpendicular and in-plane directions [26]. Indeed, a large orbital magnetic moment perpendicular to the films (0.08-0.1 μ_B/Ru) below T_C has been reported in $SrRuO_3$ films on $SrTiO_3$ [24,25]. Recently, a polarized neutron diffraction experiment revealed the unexpected large magnetic moment of oxygen, which contributes 30% of the total magnetization in the case of bulk $SrRuO_3$ [27]. Besides, Jeong *et al*. have reported a metal-insulator transition caused by a weakened Ru 4*d* t_{2g}-O 2*p* hybridization near $SrRuO_3/SrTiO_3$ interfaces [28]. These results

highlight the importance of the O 2*p* states for understanding the perpendicular magnetic anisotropy and electronic structures in $SrRuO_3$ films, and the issues remain controversial. Since the controversy may partly arise from variation in sample quality in previous experiments, it is vitally important to investigate the element-specific electronic structures and magnetic properties using very high-quality $SrRuO_3/SrTiO_3$ films.

The residual resistivity ratio (RRR), defined as the ratio of the longitudinal resistivity ρ at 300 K [ρ(300 K)] and $T\rightarrow0$ K [$\rho(T\rightarrow0$ K)] (T: temperature), is an excellent measure to gauge the purity of a metallic system: the quality of single-crystalline $SrRuO_3$ thin films. High RRR values are essential for exploring intrinsic electronic states. In particular, $SrRuO_3$ thin films with RRR values above 20 have enabled observations of dispersive quasiparticle peaks near the Fermi level (E_F) by angle-resolved photoemission spectroscopy [13] as well as quantum oscillations of Weyl fermions [18,29,30] and trivial Ru 4*d* electrons [14] via electrical resistivity [i.e., Shubnikov-de Haas (SdH) oscillations] measurements. Thus, ultra-high-quality $SrRuO_3/SrTiO_3$ films with very high RRR values could provide promising opportunities to comprehend the perpendicular magnetic anisotropy in this system.

In this study, we investigated the Ru 4*d* and O 2*p* electronic structure and magnetic properties using the ultra-high-quality $SrRuO_3$ films grown on $SrTiO_3$ substrates by soft X-ray photoemission spectroscopy (SX-PES), soft X-ray absorption spectroscopy (XAS), and X-ray magnetic circular dichroism (XMCD). To characterize the element-specific magnetic properties and the hybridization strength between the Ru 4*d* and O 2*p* orbitals, both Ru $M_{2,3}$-edge and O *K*-edge absorptions were used in XAS and XMCD measurements. To form $SrRuO_3$ with quality exceeding current levels, we employed our recently developed machine-learning-assisted molecular beam epitaxy (MBE) [31]. The

ultra-high-quality $SrRuO_3$ film, having the highest RRR of 86, allows to access intrinsic properties of $SrRuO_3$. We found large orbital magnetic moments of oxygen ions accompanied by strong orbital hybridization of the O 2*p* states with the spin-polarized Ru 4*d* t_{2g} states. The film also shows single-domain perpendicular magnetization with an almost ideal remanent magnetization ratio of 0.97.

II. EXPERIMENT

We grew high-quality epitaxial $SrRuO_3$ films with a thickness of 63 nm on the (001) $SrTiO_3$ substrates in a custom-designed MBE setup equipped with multiple e-beam evaporators for Sr and Ru. The growth parameters were optimized by Bayesian optimization, a machine learning technique for parameter optimization [31–33], with which we achieved RRR = 86. The growth temperature was 772°C. We precisely controlled the elemental fluxes, even for elements with high melting points, e.g., Ru (2250°C), by monitoring the flux rates with an electron-impact-emission-spectroscopy sensor, which were fed back to the power supplies for the e-beam evaporators. The Ru and Sr fluxes were 0.365 and 0.980 Å/s, respectively, corresponding to Ru-rich conditions. Excessive Ru is known to be desorbed from the growth surface by forming volatile species such as RuO_4 and RuO_3 under an oxidizing atmosphere, leading to stoichiometric films [10,11]. The growth rate of 1.05 Å/s was deduced from the thickness calibration of the film using cross-sectional scanning transmission electron microscopy (STEM). This growth rate agrees very well with the value of 1.08 Å/s estimated from the flux rate of Sr, confirming the accuracy of the film thickness and thus the absolute values of the resistivity, conductivity, and magnetic moment. The oxidation during growth was carried out with a mixture of ozone (O_3) and O_2 gas (~15% O_3 + 85% O_2), which was

introduced at a flow rate of ~2 sccm through an alumina nozzle pointed at the substrate. The nozzle-to-substrate distance was 15 mm. Further information about the MBE setup and preparation of the substrates is available elsewhere [34–36].

For the magnetotransport measurements, we first deposited Ag electrodes on a $SrRuO_3$ surface. Then, we patterned the samples into 200 × 350 μm^2 Hall bar structures by photolithography and Ar ion milling. Resistivity was measured using the four-probe method at 100 μA in a Physical Property Measurement System (PPMS) DynaCool sample chamber equipped with a rotating sample stage. Low-noise measurements were performed by an AC analog lock-in technique below 1 K, for which the sample was cooled down in a ^{3}He–^{4}He dilution refrigerator. The magnetization measurements were performed with a Quantum Design MPMS3 superconducting quantum interference device-vibrating sample magnetometer (SQUID-VSM) using a quartz sample holder.

The sample was transferred in the air to the helical undulator beamline BL23SU of SPring-8 [37-40] to perform the SX-PES, XAS, and XMCD measurements. The monochromator resolution $E/\Delta E$ was about 10,000. The beam spot size was 200 × 100 μm^2 [40]. For the XMCD measurements, absorption spectra for circularly polarized X rays with the photon helicity parallel (μ^+) and antiparallel (μ^-) to the spin polarization were obtained by reversing the photon helicity at each photon energy $h\nu$ and recorded in the total-electron-yield (TEY) mode. The μ^+ and μ^- spectra at the Ru $M_{2,3}$ edges and O K edge were taken for both positive and negative applied magnetic fields and averaged to eliminate spurious dichroic signals. External magnetic fields were applied perpendicular to the sample surface ([001] direction of the $SrTiO_3$ substrate). The sample temperature was varied between 6.5 and 200 K. For estimation of the integrated values of the XAS spectra at the Ru $M_{2,3}$ edge, hyperbolic tangent functions were subtracted from the spectra

as background. The sample was kept at 20 K under an ultra-high vacuum better than 10^{-8} Pa during the PES measurements. The total energy resolution was ~150 meV. The position of the Fermi level (E_F) was determined by measuring the Fermi cutoff of evaporated gold in electrical contact with the samples.

III. RESULTS AND DISCUSSION

Figures 1(a) and 1(b) show RHEED patterns of the $SrRuO_3$ surface, in which very sharp streaks with Kikuchi lines and higher-order Laue patterns can be clearly seen. This indicates that a high-quality $SrRuO_3$ layer was epitaxially grown in a two-dimensional growth mode. Figures 1(c) and 1(d) show high-angle annular dark-field STEM (HAADF-STEM) and annular bright-field STEM (ABF-STEM) images of the $SrRuO_3$ film. $SrRuO_3$ grew epitaxially on a (001) $SrTiO_3$ substrate with an abrupt substrate/film interface, as expected from the RHEED patterns. The $SrRuO_3$ film is compressively strained because the lattice constant of the $SrTiO_3$ substrate (3.905 Å) is ~0.6% smaller than the pseudocubic bulk lattice constant of $SrRuO_3$ [31].

The resistivity ρ vs. temperature T curve of the $SrRuO_3$ film shows a clear kink at 152 K [Fig. 2(a)]. The kink corresponds to the T_C where the ferromagnetic transition occurs, and spin-dependent scattering is suppressed [8]. With a residual resistivity $\rho(T \rightarrow 0$ K) of 2.18 μΩ·cm and an RRR of 86, the $SrRuO_3$ film grown by machine-learning-assisted MBE is superior to those prepared by any other method [7,8]. As shown in the inset in Fig. 1(a), below 20 K, the $SrRuO_3$ film showed a T^2 scattering rate ($\rho \propto T^2$) that is expected for a Fermi liquid, in which electron-electron scattering dominates the transport and carriers are described as Landau quasiparticle [8,14,41]. In this Fermi liquid temperature range, quantum lifetimes long enough to observe quantum oscillations are

achieved, as evidenced by the observation of the SdH oscillations of Weyl fermions with low frequencies of 25-32 T [Fig. 2(b)] [29] and those of trivial Ru 4*d*-O 2*p* band electrons with high frequencies of 360 and 3400-3800 T [inset in Fig. 2(b)] [13,14,29] (see also the Supplemental Material [42]).

To elucidate the electronic structure, we performed SX-PES measurements on the $SrRuO_3$ film. Figure 3(a) shows the Ru 3*d* core-level spectrum of the $SrRuO_3$ film taken with $h\nu$ = 1200 eV. Here, the peaks at 285.6 and 278.6 eV were assigned to C 1*s* (from air contamination at the surface) and Sr $3p_{1/2}$ [28,43,44] signals. In the Ru 3*d* spectrum, the Ru $3d_{5/2}$ component is composed of a well-screened (WS) peak (281.4 eV) and a poorly-screened (PS) peak (282.9 eV). The WS peak results from the screening of the Ru 3*d* core-hole state by conduction electrons [43,45]. Notably, our $SrRuO_3$ film shows a prominent and sharp WS peak compared with the previous studies, where the WS peaks have been observed only as a small shoulder of the PS peak or with a comparable height to the PS peak [28,43]. It should be mentioned here that this comparison may not be straightforward because the intensity of the WS peak probably depends on photon energy (probing depth) and measurement temperature as observed in perovskite manganites [46,47].” To further scrutinize this point, the spectrum was fitted to a combination of Voigt and asymmetric Gaussian functions. As shown in Fig. 3(b), the fitting well reproduces the Ru $3d_{5/2}$ and Sr 3*p* structures. In accordance with the spectral line shape of the Ru 3*d* spectrum, the WS peak is prominent rather than the PS one. This means that a Ru 3*d* core-hole state created by the photoemission process is well screened by the conduction electrons, which is consistent with the good metallic conductivity of our $SrRuO_3$ film. Moreover, there is a possibility that the Weyl fermions also contribute to this screening. The concentration of conduction electrons is related to the density of states

near E_F. Figure 3(c) shows the valence band spectrum taken with $h\nu$ = 600 eV. The intense coherent peak originating from the Ru 4*d* states near the E_F is observed. These observations of the sharp WS peak in the Ru $3d_{5/2}$ core-level spectrum and the coherent peak at E_F in the valence-band spectrum provide spectral evidence for the good metallicity of the $SrRuO_3$ film.

To get detailed insights into the orbital hybridization and the perpendicular magnetic anisotropy, we carried out XAS and XMCD measurements, which are tools sensitive to the local electronic structure and element-specific magnetic properties in magnetic materials [48-52]. Figure 4(a) shows the Ru $M_{2,3}$ XAS and XMCD spectra of the $SrRuO_3$ film at 6.5 K with a magnetic field of $\mu_0 H$ = 0 T. The spectra were measured after the application of $\mu_0 H$ = 2 T that is enough high to saturate the magnetization, and hence, the XMCD signals originate from the remanent-spontaneous magnetization. Here, μ^+ and μ^- denote the absorption coefficients for the photon helicities parallel and antiparallel to the Ru 4*d* majority spin direction, respectively. The absorption peaks at 464 and 486 eV are due to transitions from the Ru $3p_{3/2}$ and $3p_{1/2}$ core levels into the Ru 4*d* band [53]. Other structures located around 478 and 499 eV are attributed to transitions into Ru 5*s* states [24]. The peak position of the M_3-edge XMCD is lower than that of the M_3-edge XAS, indicating that the XMCD and XAS peaks come from the transitions to the Ru 4d t_{2g} and e_g bands, respectively, and only the Ru 4*d* t_{2g} states near the E_F have spin polarization. These assignments are consistent with our previous density functional theory (DFT) calculations [29], in which the half-metallic Ru 4*d* t_{2g} states cross the E_F.

We determined the orbital magnetic moment m_{orb} and the spin magnetic moment m_{spin} of the Ru^{4+} 4*d* states using the XMCD sum rules as follows [48-50]:

$$m_{\mathrm{orb}} = -\frac{4(10-n_{4d})}{3r}\int_{M_2+M_3}(\mu^+ - \mu^-)dE,$$

$$m_{\mathrm{spin}} + 7m_{\mathrm{T}} = -\frac{2(10-n_{4d})}{r}\left[\int_{M_3}(\mu^+ - \mu^-)dE - 2\int_{M_2}(\mu^+ - \mu^-)dE\right].$$

Here, $r = \int_{M_2+M_3}(\mu^+ + \mu^-)dE$, and n_{4d} is the number of electrons in 4*d* orbitals, which is assumed to be four. For ions in octahedral symmetry, the magnetic dipole moment m_{T} is a small number and can be neglected compared to m_{spin} [54]. Using the XMCD spectra taken with a magnetic field of $\mu_0 H = 2$ T at 6.5 K [Fig. 4(b)], we estimated the $m_{\mathrm{spin}} = 0.85\ \mu_{\mathrm{B}}/\mathrm{Ru}$ and $m_{\mathrm{orb}} = 0.07\ \mu_{\mathrm{B}}/\mathrm{Ru}$. The orbital magnetic moment relative to the spin magnetic moment, $m_{\mathrm{orb}}/m_{\mathrm{spin}}$, is 0.08, consistent with the reported value for $SrRuO_3$ films grown on $SrTiO_3$ (001) substrates [24,25]. The total magnetic moment, $M = m_{\mathrm{spin}} + m_{\mathrm{orb}} = 0.92$, is smaller than the saturation magnetization measured with a superconducting quantum interference device magnetometer (1.25 $\mu_{\mathrm{B}}/\mathrm{Ru}$) [31] (see also Fig. 8 later). This slight discrepancy may come from the magnetization of the O 2*p* electrons, which should be induced by orbital hybridization of the O 2*p* states with the spin-polarized Ru 4*d* states [27]. As described later, indeed, the substantial orbital magnetic moment of the O 2*p* states was verified from the O 1*s* XMCD spectrum.

Figure 5(a) shows the temperature-dependent (6.5 – 200 K) Ru $M_{2,3}$-edge XMCD spectra with a magnetic field $\mu_0 H = 0$ or 2 T. The XMCD intensities decrease with increasing *T* and drop above T_{C} (152 K), reflecting the ferromagnetic to paramagnetic transition. Figure 5(b) shows the XMCD spectra normalized at the Ru M_2 edge. Below T_{C}, the normalized XMCD spectra are identical to each other, indicating that $m_{\mathrm{orb}}/m_{\mathrm{spin}}$ stays constant below T_{C}. In contrast, the normalized Ru M_3-edge intensity in the paramagnetic state is smaller than those in the ferromagnetic state [Fig. 5(b)]. Using the

XMCD spectra at 200 K shown in Fig. 5(c), we estimated the m_{spin} = 0.037∓0.01 μ_{B}/Ru and m_{orb} = 0∓0.01 μ_{B}/Ru in the paramagnetic state. The total magnetic moment drops above T_{C}, and m_{orb} is quenched within the accuracy of the measurements, indicating that the Ru^{4+} states are in the low-spin $S = 1$ [t_{2g}^4 (3 ↑, 1 ↓)] paramagnetic state ($2\sqrt{S(S+1)}$ = 2.83 μ_{B}/Ru). This is consistent with the reported experimental effective moment of bulk $SrRuO_3$ above T_{C} (~2.6 μ_{B}/Ru) [2,55].

To clarify the unoccupied electronic states hybridized with the O 2*p* orbitals, we measured the O 1*s* XAS and XMCD spectra [Fig. 6]. The O 1*s* XAS spectra of transition metal oxides represent the unoccupied transition metal 4*d* and 5*s*/5*p* states, as well as the other conduction-band states via the hybridization with the O 2*p* states [56]. The absorption peak at 529 eV comes from transitions into the Ru 4*d* t_{2g} states, and the transitions to the Ru 4*d* e_g states appear in the energy range of 530–534.5 eV [57]. The transitions to the Sr 4*d* states and the Ru 5*s* states are observed in the range of 534.5–540 eV and 540–546 eV [43,57,58], respectively. The energy difference between the Ru 4*d* t_{2g} peak and the Ru 5*s* peak (~14.5 eV) is consistent with that in the Ru $M_{2,3}$-edge XAS and XMCD spectra (~14 eV) [Fig. 4(a)]. The O 1*s* XAS spectrum of the ultra-high-quality $SrRuO_3$ film exhibits sharper peaks than other $SrRuO_3$ films on $SrTiO_3$ [28,43] and bulk $SrRuO_3$ [56,57,58] with similar overall features. Notably, the intensity ratio of the Ru 4*d* t_{2g} peak to the Sr 4*d* peak (1.55) is larger than those in other $SrRuO_3$ films on $SrTiO_3$ and bulk $SrRuO_3$ (0.8-1.3) [28,43,56-58]. The smaller Ru 4*d* t_{2g} peak in previous studies may come from the less itinerant nature (shorter lifetimes) of the quasiparticles in the hybridized O 2*p*-Ru 4*d* t_{2g} states crossing the E_{F}, as a consequence of, for instance, disorder-induced localization. The localization comes from hybridization between

different basis states caused by the disorder when seen as a perturbation to the Hamiltonian in the zero-disorder limit [59].

The substantial orbital magnetic moment of the O 2*p* states induced by the hybridization with the Ru 4*d* t_{2g} states was observed from the O 1*s* XMCD spectrum (Fig. 6). The sizeable negative XMCD structure was observed only in the energy range corresponding to Ru 4*d* t_{2g}, indicating that the influence of the magnetization due to hybridizations with the states other than Ru 4*d* t_{2g} is negligibly small. This is consistent with our previous DFT calculations [29], in which the half-metallic bands crossing the E_F are formed by the Ru 4*d* t_{2g} states hybridized with the O 2*p* states. The O 1*s* XMCD peak intensity at 529.1 eV divided by the O 1*s* XAS peak intensity at 529 eV (0.13) is twice as large as that of bulk polycrystalline $SrRuO_3$ (~0.06) [58]. Since the energy-integrated intensity of the O 1*s* XMCD is proportional to the orbital magnetic moment of the O 2*p* states [48], the larger O 1*s* XMCD intensity indicates the large orbital magnetic moment of the O 2*p* states in the ultra-high-quality $SrRuO_3$ film. According to P. Bruno [26], the larger orbital magnetic moment perpendicular to the film should lead to perpendicular magnetic anisotropy, as confirmed by XMCD for several systems, including Co thin films sandwiched by Au(111) [60] and FePt [61]. Thus, the large orbital magnetic moments of the hybridized O 2*p*-Ru 4*d* t_{2g} states in ultra-high-quality $SrRuO_3$ films will lead to the strong perpendicular magnetic anisotropy. Indeed, an epitaxial $SrRuO_3$ film, whose RRR is over 50, on $SrTiO_3$ showed the largest perpendicular magnetic anisotropy among $SrRuO_3$ films on $SrTiO_3$ reported at the time [31].

Figure 7 shows XMCD-*H* curves measured at the Ru M_3 edge (462.4 eV) for our ultra-high-quality $SrRuO_3$ film at 6.5 K. The vertical axis of the XMCD intensity at 2 T has been scaled so that it represents the sum of the total magnetic moment $M = m_{\mathrm{spin}} +$

m_{orb} of the Ru ions estimated from Fig. 4(b). The rectangular hysteresis with the small coercive field H_c of ~0.02 T means that the easy direction of magnetization is perpendicular to the film surface, as is usually the case with compressively strained $SrRuO_3$ films on $SrTiO_3$ substrates [8,29,31]. The H_c of ~0.02 T is smaller than those previously reported for $SrRuO_3$ films (H_c > 0.1 T) [8,29,31]. Since the magnetic domains tend to be pinned by grain boundaries and other defects, the small H_c stems from the higher crystallinity of our film. Notably, the ratio of remanent magnetization to saturation magnetization, estimated by the M values at 0 and ±2 T in Fig. 7, is almost an ideal value of 0.97, indicating the single-domain perpendicular magnetization. To our knowledge, this is the highest value reported for all oxides [62-64]. We note that, for accurate determination of the remanent magnetization ratio of magnetic thin films, XMCD is adequate because it is free from the diamagnetic signal from the substrate. The nearly ideal perpendicular magnetization mentioned above, which stems from the large orbital magnetic moment of the O 2*p*-Ru 4*d* hybridized states as well as less grain boundary and defect densities, is beneficial for spintronics applications; with larger perpendicular magnetization, the magnetic configuration is thermally more stable, and the spin-transfer switching current is lower [65,66].

To verify the perpendicular magnetic anisotropy, we carried out magnetization measurements by SQUID. Figure 8 shows the magnetic moment vs. H curves for the $SrRuO_3$ film at 6 K with magnetic fields applied to the out-of-plane [001] (blue circles) and in-plane [100] (purple circles) directions of the $SrTiO_3$ substrate. The saturation magnetization along the out-of-plane [001] direction was 1.24 μ_B/Ru. In contrast, the magnetization along the in-plane [100] direction did not saturate at 2 T. This confirms that the easy direction of magnetization was perpendicular to the film surface. The

remanent magnetization ratio for the out-of-plane [001] direction estimated from the SQUID data (0.6) is lower than that estimated from the XMCD-*H* curve (0.97). This discrepancy probably comes from the magnetization of the $SrTiO_3$ substrate in the SQUID measurements. The magnetization curve for the $SrTiO_3$ substrate at 1.9 K reported in our previous study [36] shows the nonlinear magnetic response near the zero magnetic field. The nonlinear magnetic response indicates the existence of magnetic impurities in the $SrTiO_3$ substrate. The overlapping of the nonlinear magnetic response from the $SrTiO_3$ substrate causes underestimation of the remanent magnetization in SQUID measurements. In contrast, we can accurately determine remanent magnetization ratios of magnetic thin films by XMCD-*H* curves since they are free from the magnetic signal from the substrate, as described above. The H_c value for the out-of-plane [001] direction obtained from the SQUID data (~0.035 T) is larger than that obtained from the XMCD-*H* curve (~0.02 T). This discrepancy may come from the difference in the magnetization process between the surface and the bulk. Since the typical probing depth of the XMCD measurement is 2-3 nm in the total electron yield mode [37], the magnetization process may be influenced by electronic states at the surface. Whichever value we use, the H_c value is the smallest reported so far [8,29,31].

IV. CONCLUSIONS

We have investigated the Ru 4*d* and O 2*p* electronic structure and magnetic properties of the ultra-high-quality $SrRuO_3$ film on $SrTiO_3$ grown by machine-learning-assisted MBE. The thusly prepared $SrRuO_3$ film, with a residual resistivity ρ(T→0 K) of 2.18 μΩ·cm and a RRR of 86, is superior to those obtained by any other method, allowing access the intrinsic properties of $SrRuO_3$. We observed the prominent well-

screened peak in the Ru $3d_{5/2}$ core-level spectrum and the coherent Ru 4*d* t_{2g} peak at E_F by SX-PES. Together with quantum oscillations in the resistivity, the highly itinerant nature (long quantum lifetime) of the quasiparticles in the Ru 4*d* t_{2g}-O 2*p* hybridized bands crossing the E_F is confirmed. We also revealed large orbital magnetic moments of oxygen ions and the strong orbital hybridization of the O 2*p* states with the spin-polarized Ru 4*d* t_{2g} states. The O 2*p*-Ru 4*d* t_{2g} hybridization in the ultra-high-quality $SrRuO_3$ film is more significant than those in other $SrRuO_3$ films on $SrTiO_3$ and in bulk $SrRuO_3$ [28,43,56-58], and this strong O 2*p*-Ru 4*d* t_{2g} hybridization is responsible for the high itinerancy of the quasiparticles at around the Fermi level. The ultra-high-quality $SrRuO_3$ film shows single-domain perpendicular magnetization with an almost ideal remanent magnetization ratio of 0.97. These results provide important insights into the relevance between the orbital hybridization and perpendicular magnetic anisotropy in $SrRuO_3/SrTiO_3$ systems and for applying $SrRuO_3$ as a metallic ferromagnetic oxide electrode for hetero-epitaxially grown spintronic devices.

ACKNOWLEDGMENTS

This work was partially supported by JST-CREST (JPMJCR18T5) and the Spintronics Research Network of Japan (Spin-RNJ). This work was performed under the Shared Use Program of Japan Atomic Energy Agency (JAEA) Facilities (Proposal No. 2020A-E18) supported by JAEA Advanced Characterization Nanotechnology Platform as a program of ”Nanotechnology Platform“ of the Ministry of Education, Culture, Sports, Science and Technology (MEXT) (Proposal No. JPMXP09A20AE0018). The experiment at SPring-8 was approved by the Japan Synchrotron Radiation Research Institute (JASRI) Proposal Review Committee (Proposal No. 2020A3841).

AUTHORS' CONTRIBUTIONS

Y.K.W. conceived the idea, designed the experiments, and directed and supervised the project. M.K. and Y.K.W. planned the synchrotron experiments. Y.K.W. and Y.K. grew the samples. Y.K.W. carried out the sample characterizations. K.T., Y.K.W., and H.I. carried out the magnetotransport measurements. Y.K.W., M.K., Y.Tak., T.T., and R.O. carried out the XMCD measurements. M.K. and S.-I.F. carried out the X-ray PES measurements. Y.K.W. and M.K. analyzed and interpreted the data. Y.K.W. wrote the paper with input from all authors.

DATA AVAILABILITY

Data that support the findings of this study are available from the corresponding author upon reasonable request.

References

[1] J. J. Randall and R. Ward, The Preparation of Some Ternary Oxides of the Platinum Metals, J. Am. Chem. Soc. **81**, 2629 (1959).

[2] J. M. Longo, P. M. Raccah, and J. B. Goodenough, Magnetic Properties of $SrRuO_3$ and $CaRuO_3$, J. Appl. Phys. **39**, 1327 (1968).

[3] R. J. Bouchard and J. L. Gillson, Electrical properties of $CaRuO_3$ and $SrRuO_3$ single crystals, Mater. Res. Bull. **7**, 873 (1972).

[4] L. Klein and J. S. Dodge, C. H. Ahn, J. W. Reiner, L. Mieville, T. H. Geballe, M. R. Beasley, and A. Kapitulnik, Transport and magnetization in the badly metallic itinerant ferromagnet $SrRuO_3$, J. Phys. Condens. Matter **8**, 10111, (1996).

[5] C. B. Eom, R. J. Cava, R. M. Fleming, J. M. Phillips, R. B. van Dover, J. H. Marshall, J. W. P. Hsu, J. J. Krajewski, and W. F. Peck, Jr., Single-Crystal Epitaxial Thin Films of the Isotropic Metallic Oxides $Sr_{1-x}Ca_xRuO_3$ ($0 \leq x \leq 1$), Science **258**, 1766, (1992).

[6] X. D. Wu, S. R. Foltyn, R. C. Dye, Y. Coulter, and R. E. Muenchausen, Properties of epitaxial $SrRuO_3$ thin films, Appl. Phys. Lett. **62**, 2434 (1993).

[7] M. Izumi, K. Nakazawa, Y. Bando, Y. Yoneda, and H. Terauchi, Magnetotransport of $SrRuO_3$ Thin Film on $SrTiO_3$ (001), J. Phys. Soc. Jpn. **66**, 3893 (1997).

[8] G. Koster, L. Klein, W. Siemons, G. Rijnders, J. S. Dodge, C.-B. Eom, D. H. A. Blank, M. R. Beasley, Structure, physical properties, and applications of $SrRuO_3$ thin films, Rev. Mod. Phys. **84**, 253 (2012).

[9] D. Kan, M. Mizumaki, T. Nishimura, and Y. Shimakawa, Orbital Magnetic Moments in Strained $SrRuO_3$ Thin Films, Phys. Rev. B, **94**, 214420, (2016).

[10] H. P. Nair, Y. Liu, J. P. Ruf, N. J. Schreiber, S.-L. Shang, D. J. Baek, B. H. Goodge, L. F. Kourkoutis, Z.-K. Liu, K. M. Shen, and D. G. Schlom, Synthesis Science of $SrRuO_3$ and $CaRuO_3$ Epitaxial Films with High Residual Resistivity Ratios, APL Mater. **6**, 046101 (2018).

[11] W. Siemons, G. Koster, A. Vailionis, H. Yamamoto, D. H. A. Blank, and M. R. Beasley, Dependence of the electronic structure of $SrRuO_3$ and its degree of correlation on cation off-stoichiometry, Phys. Rev. B **76**, 075126 (2007).

[12] J. Thompson, J. Nichols, S. Lee, S. Ryee, J. H. Gruenewald, J. G. Connell, M. Souri, J. M. Johnson, J. Hwang, M. J. Han, H. N. Lee, D.-W. Kim, and S. S. A. Seo, Enhanced metallic properties of $SrRuO_3$ thin films via kinetically controlled pulsed laser epitaxy, Appl. Phys. Lett. **109**, 161902 (2016).

[13] D. E. Shai, C. Adamo, D. W. Shen, C. M. Brooks, J. W. Harter, E. J. Monkman, B. Burganov, D. G. Schlom, and K.M. Shen, Quasiparticle mass enhancement and temperature dependence of the electronic structure of ferromagnetic $SrRuO_3$ thin films, Phys. Rev. Lett. **110**, 087004 (2013).

[14] A. P. Mackenzie, J. W. Reiner, A. W. Tyler, L. M. Galvin, S. R. Julian, M. R. Beasley, T. H. Geballe, and A. Kapitulnik, Observation of quantum oscillations in the electrical resistivity of $SrRuO_3$, Phys. Rev. B **58**, R13318 (1998).

[15] D. C. Worledge and T. H. Geballe, Negative Spin-Polarization of $SrRuO_3$, Phys. Rev. Lett. **85**, 5182 (2000).

[16] K. S. Takahashi, A. Sawa, Y. Ishii, H. Akoh, M. Kawasaki, and Y. Tokura, Inverse tunnel magnetoresistance in all-perovskite junctions of $La_{0.7}Sr_{0.3}MnO_3/SrTiO_3/SrRuO_3$, Phys. Rev. B **67**, 094413 (2003).

[17] Z. Li, S. Shen, Z. Tian, K. Hwangbo, M. Wang, Y. Wang, F. M. Bartram, L. He, Y.

Lyu, Y. Dong, G. Wan, H. Li, N. Lu, J. Zang, H. Zhou, E. Arenholz, Q. He, L. Yang, W. Luo, and P. Yu, Reversible manipulation of the magnetic state in $SrRuO_3$ through electric-field controlled proton evolution, Nat. Commun. **11**, 184 (2020).

[18] S. K. Takada, Y. K. Wakabayashi, Y. Krockenberger, S. Ohya, M. Tanaka, Y. Taniyasu, and H. Yamamoto, Thickness-dependent quantum transport of Weyl fermions in ultra-high-quality $SrRuO_3$ films, Appl. Phys. Lett. **118**, 092408 (2021).

[19] Y. K. Wakabayashi, S. K. Takada, Y. Krockenberger, K. Takiguchi, S. Ohya, M. Tanaka, Y. Taniyasu, and H. Yamamoto, Structural and transport properties of highly Ru-deficient $SrRu_{0.7}O_3$ thin films prepared by molecular beam epitaxy: Comparison with stoichiometric $SrRuO_3$, AIP advances **11**, 035226 (2021).

[20] Y. K. Wakabayashi, S. K. Takada, Y. Krockenberger, Y. Taniyasu, and H. Yamamoto, Wide-Range Epitaxial Strain Control of Electrical and Magnetic Properties in High-Quality $SrRuO_3$ Films, ACS Applied Electronic Materials **3**, 2712 (2021).

[21] H. Boschker, T. Harada, T. Asaba, R. Ashoori, A. V. Boris, H. Hilgenkamp, C. R. Hughes, M. E. Holtz, L. Li, D. A. Muller, H. Nair, P. Reith, X. R. Wang, D. G. Schlom, A. Soukiassian, and J. Mannhart, Ferromagnetism and Conductivity in Atomically Thin $SrRuO_3$, Phys. Rev. X **9**, 011027 (2019).

[22] L. Liu, Q. Qin, W. Lin, C. Li, Q. Xie, S. He, X. Shu, C. Zhou, Z. Lim, J. Yu, W. Lu, M. Li, X. Yan, S.J. Pennycook, and J. Chen, Current-induced magnetization switching in all-oxide heterostructures, Nat. Nanotechnol. **14**, 939 (2019).

[23] L. Klein, J. S. Dodge, T. H. Geballe, A. Kapitulnik, A. F. Marshall, L. Antognazza, and K. Char, Perpendicular magnetic anisotropy and strong magneto-optic properties of $SrRuO_3$ epitaxial films, Appl. Phys. Lett. **66**, 2427 (1995).

[24] K. Ishigami, K. Yoshimatsu, D. Toyota, M. Takizawa, T. Yoshida, G. Shibata, T.

Harano, Y. Takahashi, T. Kadono, V. K. Verma, V. R. Singh, Y. Takeda, T. Okane, Y. Saitoh, H. Yamagami, T. Koide, M. Oshima, H. Kumigashira, and A. Fujimori, Thickness-dependent magnetic properties and strain-induced orbital magnetic moment in $SrRuO_3$ thin films, Phys. Rev. B **92**, 064402 (2015).

[25] A. J. Grutter, F. J. Wong, E. Arenholz, A. Vailionis, and Y. Suzuki, Evidence of high-spin Ru and universal magnetic anisotropy in $SrRuO_3$ thin films, Phys. Rev. B **85**, 134429 (2012).

[26] P. Bruno, Tight-binding approach to the orbital magnetic moment and magnetocrystalline anisotropy of transition-metal monolayers, Phys. Rev. B **39**, 865 (1989).

[27] S. Kunkemöller, K. Jenni, D. Gorkov, A. Stunault, S. Streltsov, and M. Braden, Magnetization density distribution in the metallic ferromagnet $SrRuO_3$ determined by polarized neutron diffraction, Phys. Rev. B **100**, 054413 (2019).

[28] H. Jeong, S. G. Jeong, A. Y. Mohamed, M. Lee, W. Noh, Y. Kim, J. S. Bae, W. S. Choi, and D. Y. Cho, Thickness-dependent orbital hybridization in ultrathin $SrRuO_3$ epitaxial films, Appl. Phys. Lett. **115**, 092906 (2019).

[29] K. Takiguchi, Y. K. Wakabayashi, H. Irie, Y. Krockenberger, T. Otsuka, H. Sawada, S. A. Nikolaev, H. Das, M. Tanaka, Y. Taniyasu, and H. Yamamoto, Quantum transport evidence of Weyl fermions in an epitaxial ferromagnetic oxide, Nat. Commun. **11**, 4969 (2020).

[30] S. K. Takada, Y. K. Wakabayashi, Y. Krockenberger, T. Nomura, Y. Kohama, H. Irie, K. Takiguchi, S. Ohya, M. Tanaka, Y. Taniyasu, H. Yamamoto, Quantum Limit Transport and Two-Dimensional Weyl Fermions in an Epitaxial Ferromagnetic Oxide, arXiv:2106.03292.

[31] Y. K. Wakabayashi, T. Otsuka, Y. Krockenberger, H. Sawada, Y. Taniyasu, and H. Yamamoto, Machine-learning-assisted thin-film growth: Bayesian optimization in molecular beam epitaxy of $SrRuO_3$ thin films, APL Mater. **7**, 101114 (2019).

[32] J. Snoek, H. Larochelle, and R. P. Adams, Practical Bayesian Optimization of Machine Learning Algorithms, paper presented at Advances in Neural Information Processing Systems 25, 2012, see also http://papers.nips.cc/paper/4522- practical-bayesian-optimization.

[33] Y. K. Wakabayashi, T. Otsuka, Y. Taniyasu, H. Yamamoto, and H. Sawada, Improved adaptive sampling method utilizing Gaussian process regression for prediction of spectral peak structures, Appl. Phys. Express **11**, 112401 (2018).

[34] M. Naito and H. Sato, Increase in the superconducting transition temperature by anisotropic strain effect in (001) $La_{1.85}Sr_{0.15}CuO_4$ thin films on $LaSrAlO_4$ substrates, Appl. Phys. Lett. **67**, 2557 (1995).

[35] H. Yamamoto, Y. Krockenberger, and M. Naito, Multi-source MBE with high-precision rate control system as a synthesis method sui generis for multi-cation metal oxides, J. Cryst. Growth **378**, 184 (2013).

[36] Y. K. Wakabayashi, Y. Krockenberger, N. Tsujimoto, T. Boykin, S. Tsuneyuki, Y. Taniyasu, and H. Yamamoto, Ferromagnetism above 1000 K in a highly cation-ordered double-perovskite insulator Sr_3OsO_6, Nat. Commun. **10**, 535 (2019).

[37] R. Nakajima, J. Stohr, and Y. U. Idzerda, Electron-yield saturation effects in L-edge x-ray magnetic circular dichroism spectra of Fe, Co, and Ni, Phys. Rev. B 59, 6421 (1999).

[38] A. Yokoya, T. Sekiguchi, Y. Saitoh, T. Okane, T. Nakatani, T. Shimada, H. Kobayashi, M. Takao, Y. Teraoka, Y. Hayashi, S. Sasaki, Y. Miyahara, T. Harami,

and T. A. Sasaki, Soft X-ray beamline specialized for actinides and radioactive materials equipped with a variably polarizing undulator, J. Synchrotron Rad. **5**, 10 (1998).

[39] J. Okamoto, K. Mamiya, S.-I. Fujimori, T. Okane, Y. Saitoh, Y. Muramatsu, A. Fujimori, S. Ishiwata, and M. Takano, Magnetic Circular X-ray Dichroism Study of Paramagnetic and Anti-Ferromagnetic States in $SrFeO_3$ Using a 10-T Superconducting Magnet, AIP Conf. Proc. **705**, 1110 (2004).

[40] Y. Saitoh, Y. Fukuda, Y. Takeda, H. Yamagami, S. Takahashi, Y. Asano, T. Hara, K. Shirasawa, M. Takeuchi, T. Tanaka, and H. Kitamura, Performance upgrade in the JAEA actinide science beamline BL23SU at SPring-8 with a new twin-helical undulator, J. Synchrotron Rad. **19**, 388 (2012).

[41] Y. Wang, G. Bosse, H. P. Nair, N. J. Schreiber, J. P. Ruf, B. Cheng, C. Adamo, D. E. Shai, Y. Lubashevsky, D. G. Schlom, K. M. Shen, and N. P. Armitage, Subterahertz Momentum Drag and Violation of Matthiessen's Rule in an Ultraclean Ferromagnetic $SrRuO_3$ Metallic Thin Film, Phys. Rev. Lett. **125**, 217401 (2020).

[42] See Supplemental Materials at http:/... for the analyses of the SdH oscillations.

[43] M. Takizawa, D. Toyota, H. Wadati, A. Chikamatsu, H. Kumigashira, A. Fujimori, M. Oshima, Z. Fang, M. Lippmaa, M. Kawasaki, and H. Koinuma, Manifestation of correlation effects in the photoemission spectra of $Ca_{1-x}Sr_xRuO_3$ Phys. Rev. B **72**, 060404(R) (2005).

[44] J. Shin, S. V. Kalinin, H. N. Lee, H. M. Christen, R. G. Moore, E. W. Plummer, A. P. Baddorf, Surface stability of epitaxial $SrRuO_3$ films, Surf. Sci. **581**, 118 (2005).

[45] P. A. Cox, J. B. Goodenough, P. J. Tavener, D. Telles and R. G. Egdell, The electronic

structure of $Bi_{2-x}Gd_xRu_2O_7$ and RuO_2: a study by electron spectroscopy, J. Solid State Chem. **62**, 360 (1986).

[46] K. Horiba, M. Taguchi, A. Chainani, Y. Takata, E. Ikenaga, D. Miwa, Y. Nishino, K. Tamasaku, M. Awaji, A. Takeuchi, M. Yabashi, H. Namatame, M. Taniguchi, H. Kumigashira, M. Oshima, M. Lippmaa, M. Kawasaki, H. Koinuma, K. Kobayashi, T. Ishikawa, and S. Shin, Nature of the Well Screened State in Hard X-Ray Mn 2*p* Core-Level Photoemission Measurements of $La_{1-x}Sr_xMnO_3$ Films, Phys. Rev. Lett. **93**, 236401 (2004).

[47] T. Hishida, K. Ohbayashi, M. Kobata, E. Ikenaga, T. Sugiyama, K. Kobayashi, M. Okawa, and T. Saitoh, Empirical relationship between x-ray photoemission spectra and electrical conductivity in a colossal magnetoresistive manganite $La_{1-x}SrxMnO_3$, J. Appl. Phys. **113**, 233302 (2013).

[48] B. T. Thole, P. Carra, F. Sette, and G. van der Laan, X-ray circular dichroism as a probe of orbital magnetization, Phys. Rev. Lett. **68**, 1943 (1992).

[49] C. T. Chen, Y. U. Idzerda, H. -J. Lin, N. V. Smith, G. Meigs, E. Chaban, G. H. Ho, E. Pellegrin, and F. Sette, Experimental confirmation of the X-ray magnetic circular dichroism sum rules for iron and cobalt, Phys. Rev. Lett. **75**, 152 (1995).

[50] J. Stohr and H. Konig, Determination of spin-and orbital-moment anisotropies in transition metals by angle-dependent X-ray magnetic circular dichroism, Phys. Rev. Lett. **75**, 3748 (1995).

[51] Y. K. Wakabayashi, S. Sakamoto, Y. Takeda, K. Ishigami, Y. Takahashi, Y. Saitoh, H. Yamagami, A. Fujimori, M. Tanaka, and S. Ohya, Room-temperature local ferromagnetism and its nanoscale expansion in the ferromagnetic semiconductor $Ge_{1-x}Fe_x$, Sci. Rep. **6**, 23295 (2016).

[52] Y. K. Wakabayashi, Y. Nonaka, Y. Takeda, S. Sakamoto, K. Ikeda, Z. Chi, G. Shibata, A. Tanaka, Y. Saitoh, H. Yamagami, M. Tanaka, A. Fujimori, and R. Nakane, Electronic structure and magnetic properties of magnetically dead layers in epitaxial $CoFe_2O_4/Al_2O_3/Si$ (111) films studied by x-ray magnetic circular dichroism, Phys. Rev. B **96**, 104410 (2017).

[53] K. Terai, K. Yoshii, Y. Takeda, S. I. Fujimori, Y. Saitoh, K. Ohwada, T. Inami, T. Okane, M. Arita, K. Shimada, H. Namatame, M. Taniguchi, K. Kobayashi, M. Kobayashi, and A. Fujimori, X-ray magnetic circular dichroism and photoemission studies of ferromagnetism in $CaMn_{1-x}Ru_xO_3$ thin films, Phys. Rev. B **77**, 115128 (2008).

[54] Y. Teramura, A. Tanaka, and T. Jo, Effect of Coulomb Interaction on the X-Ray Magnetic Circular Dichroism Spin Sum Rule in 3 *d* Transition Elements, J. Phys. Soc. Jpn. **65**, 1053 (1996).

[55] A. Callaghan, C. W. Moeller, and R. Ward, Magnetic interactions in ternary ruthenium oxides, Inorg. Chem. **5**, 1573 (1966).

[56] D. H. Kim, E. Lee, H. W. Kim, S. Kolesnik, B. Dabrowski, C. -J. Kang, M. Kim, B. I. Min, H. -K. Lee, J. -Y. Kim, and J. -S. Kang, Correlation between Mn and Ru valence states and magnetic phases in $SrMn_{1-x}Ru_xO_3$, Phys. Rev. B **91**, 075113 (2015).

[57] K. Fujioka, J. Okamoto, T. Mizokawa, A. Fujimori, I. Hase, M. Abbate, H. J. Lin, C. T. Chen, Y. Takeda, and M. Takano, Electronic structure of $SrRuO_3$, Phys. Rev. B **56**, 6380 (1997).

[58] J. Okamoto, T. Okane, Y. Saitoh, K. Terai, S.-I. Fujimori, Y. Muramatsu, K. Yoshii,1 K. Mamiya, T. Koide, A. Fujimori, Z. Fang, Y. Takeda, and M. Takano, Soft x-ray

magnetic circular dichroism study of $Ca_{1-x}Sr_xRuO_3$ across the ferromagnetic quantum phase transition, Phys. Rev. B **76**, 184441 (2007).

[59] S. Ashhab, O. Voznyy, S. Hoogland, E. H. Sargent, M. E. Madjet, Effect of disorder on transport properties in a tight-binding model for lead halide perovskites, Sci. Rep. **7**, 8902 (2017).

[60] D. Weller, J. Stohr, R. Nakajima, A. Carl, M. G. Samant, C. Chappert, R. Megy, P. Beauvillain, P. Veillet, and G. A. Held, Microscopic origin of magnetic anisotropy in Au/Co/Au probed with x-ray magnetic circular dichroism, Phys. Rev. Lett. **75**, 3752 (1995).

[61] S. Imada, A. Yamasaki, S. Suga, T. Shimac, and K. Takanashi, Perpendicular magnetization of $L1_0$ -ordered FePt films in the thinnest limit, Appl. Phys. Lett. **90**, 132507 (2007).

[62] C. Thiele, K. Dörr, O. Bilani, J. Rödel, and L. Schultz, Influence of strain on the magnetization and magnetoelectric effect in $La_{0.7}Sr_{0.3}MnO_3$/PMN-PT(001) (A = Sr,Ca), Phys. Rev. B **75**, 054408 (2007).

[63] T. Nagahama, Y. Matsuda, K. Tate, T. Kawai, N. Takahashi, S. Hiratani, Y. Watanabe, T. Yanase, and T. Shimada, Magnetic properties of epitaxial Fe_3O_4 films with various crystal orientations and tunnel magnetoresistance effect at room temperature, Appl. Phys. Lett. **105**, 102410 (2014).

[64] A. Omelyanchik, G. Singh, M. Volochaev, A. Sokolov, V. Rodionova, and D. Peddis, Tunable magnetic properties of Ni-doped $CoFe_2O_4$ nanoparticles prepared by the sol–gel citrate self-combustion method, J. Magn. Magn. Mater. **476**, 387 (2019).

[65] M. Kohda, A. Ohtsu, T. Seki, A. Fujita, J. Nitta, S. Mitani, and K. Takanashi, High Remanent Magnetization of $L1_0$-Ordered FePt Thin Film on MgO/(001) GaAs, Jpn.

J. Appl. Phys. **47**, 3269 (2008).

[66] S. Ikeda, K. Miura, H. Yamamoto, K. Mizunuma, H. D. Gan, M. Endo, S. Kanai, J. Hayakawa, F. Matsukura, and H. Ohno, A perpendicular-anisotropy CoFeB–MgO magnetic tunnel junction, Nat. Mater. **9**, 721 (2010).

Figures and figure captions

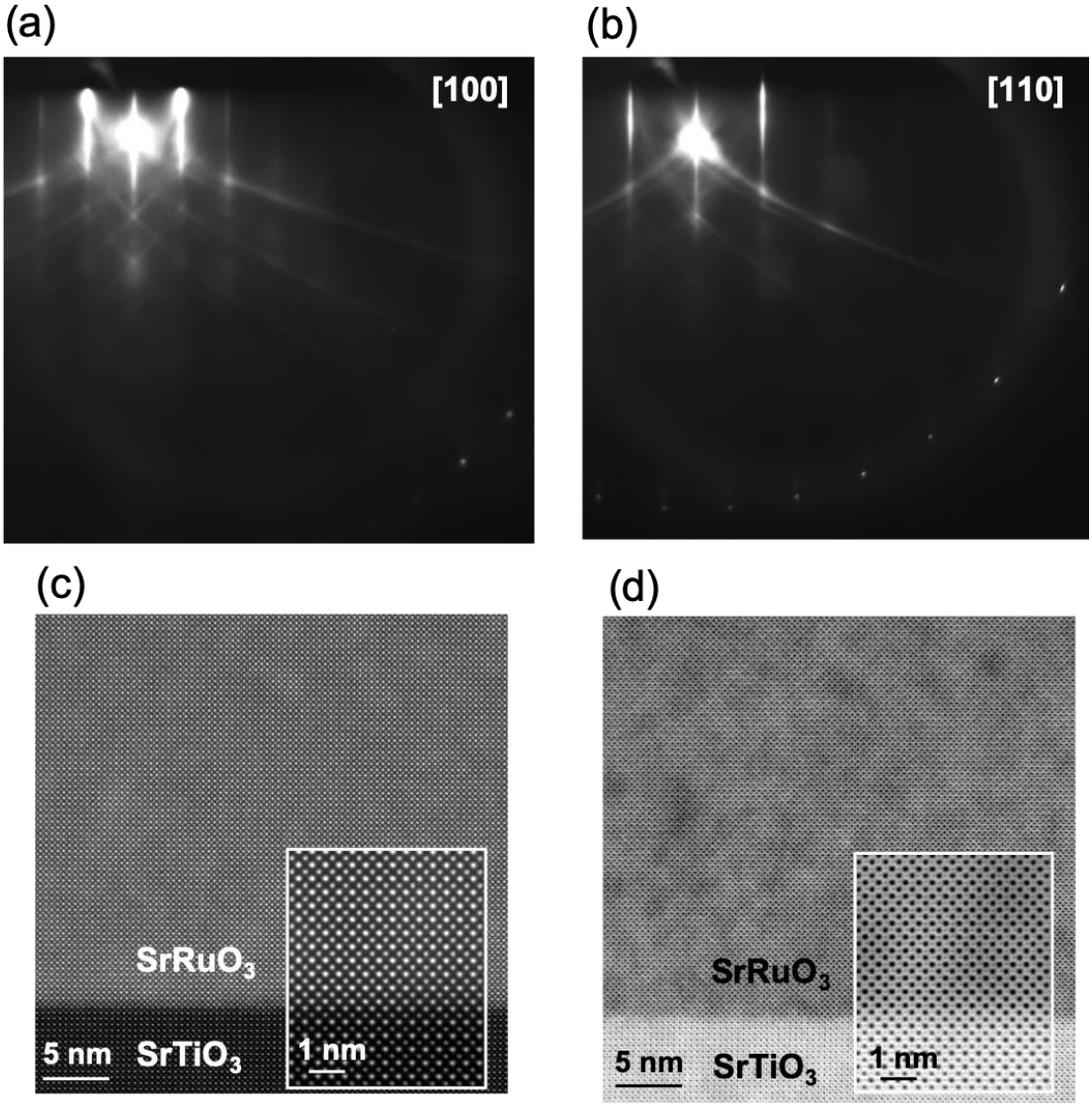

FIG. 1. RHEED patterns of a $SrRuO_3$ film taken along the (a) [100] and (b) [110] axes of the $SrTiO_3$ substrates. (c) HAADF-STEM and (d) ABF-STEM images of a $SrRuO_3$ film taken along the [100] axis of the $SrTiO_3$ substrates. The insets in (c) and (d) are magnified images near the interface.

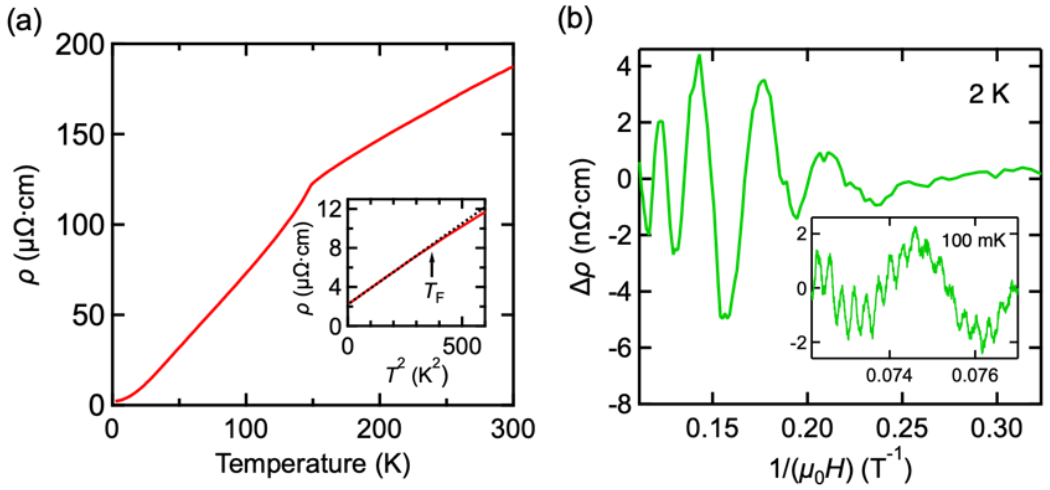

FIG. 2. (a) Temperature dependence of resistivity ρ of the $SrRuO_3$ film. The inset in (a) is a ρ versus T^2 plot with a linear fitting (black dashed line). We defined the Fermi liquid temperature range as the temperature range where the experimental ρ_{xx} and the linear fitting line in ρ_{xx} vs. T^2 are close enough to each other (< 0.1 μΩ·cm). (b) SdH oscillation measured at 2 K with $\mu_0 H$ (3 T < $\mu_0 H$ < 9 T) applied in the out-of-plane [001] direction of the $SrTiO_3$ substrate for the $SrRuO_3$ film. The inset shows SdH oscillation observed at 0.1 K with $\mu_0 H$ (13 T < $\mu_0 H$ < 14 T).

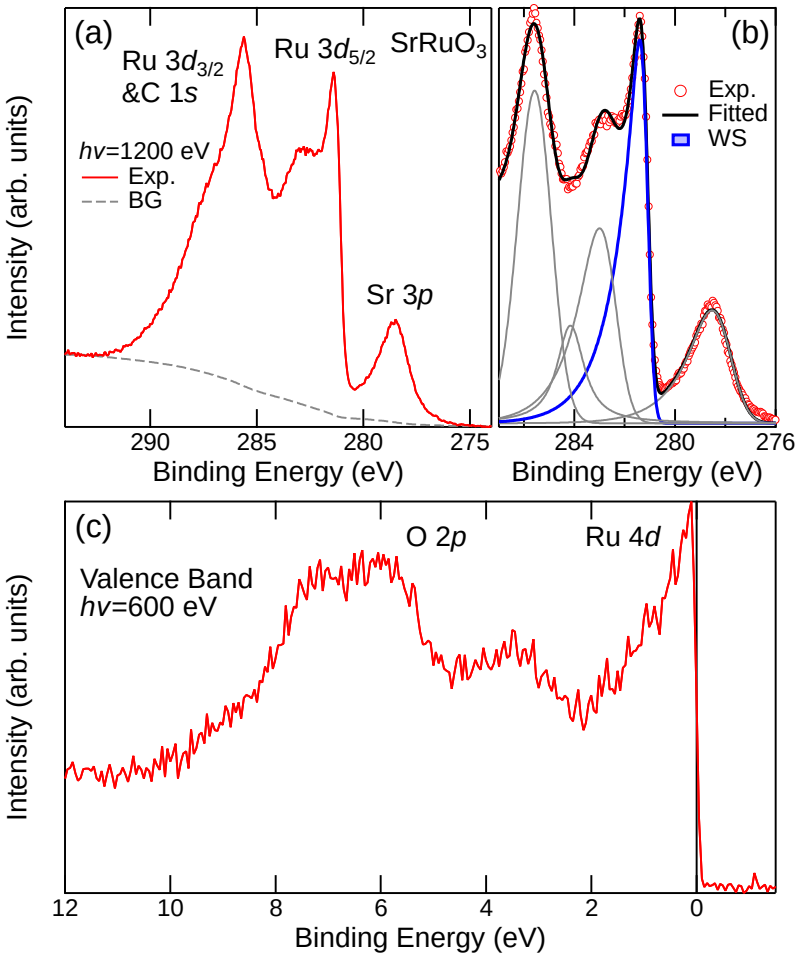

FIG. 3. SX-PES spectra of the $SrRuO_3$ film. (a) Ru 3d and Sr 3p core-level spectrum taken with the photon energy ($h\nu$) of 1200 eV at 20 K. (b) Peak fitting for the Ru 3d spectrum. WS denotes the well-screened peak. Fitting functions are Voigt and asymmetric Gaussian. (c) Valence band spectra taken with $h\nu$ of 600 eV at 20 K.

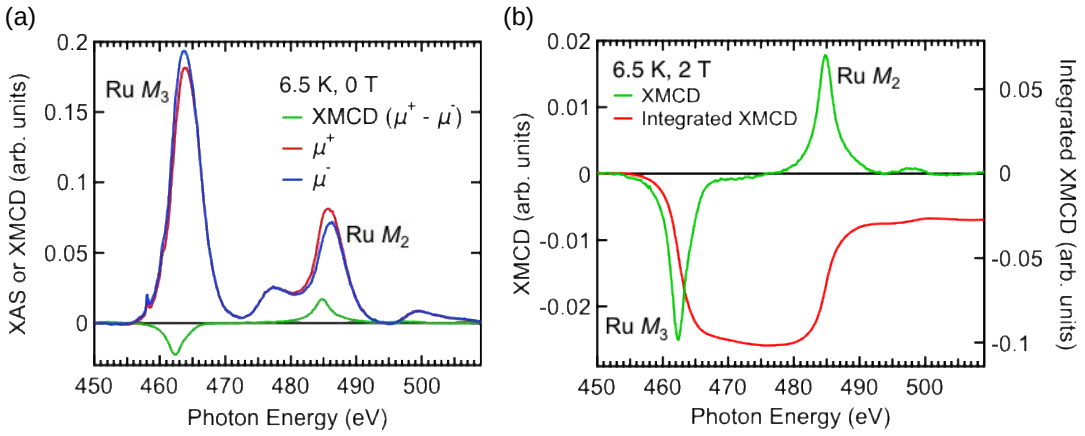

FIG. 4. (a) Ru $M_{2,3}$ edge XAS and XMCD spectra for the $SrRuO_3$ film at 6.5 K with a magnetic field $\mu_0 H$ = 0 T applied perpendicular to the film surface. The spectra were measured after the application of $\mu_0 H$ = 2 T. (b) XMCD spectra and integrated XMCD signals from 450 eV taken at 6.5 K with a magnetic field $\mu_0 H$ = 2 T applied perpendicular to the film surface.

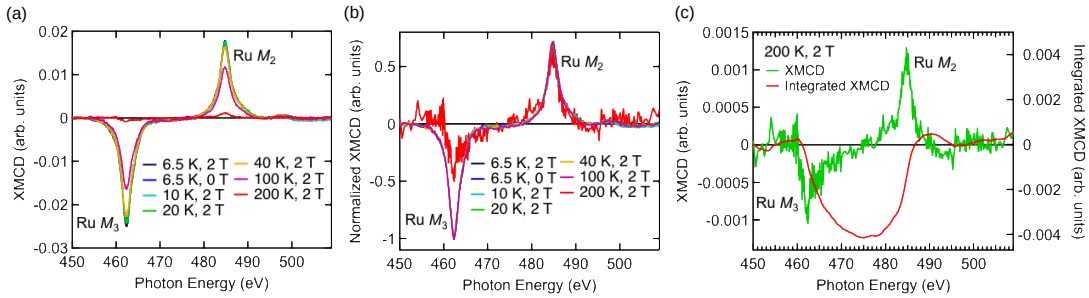

FIG. 5. (a) Ru $M_{2,3}$ edge XMCD spectra for the $SrRuO_3$ film at 6.5 to 200 K with a magnetic field $\mu_0 H = 0$ or 2 T applied perpendicular to the film surface. Here, the zero magnetic field was set after the application of $\mu_0 H = 2$ T. (b) Ru $M_{2,3}$ edge XMCD spectra normalized at 484.7 eV for the $SrRuO_3$ film at 6.5 to 200 K with a magnetic field $\mu_0 H =$ 0 or 2 T applied perpendicular to the film surface. Spectra measured at 6.5, 10, 20, 40, and 100 K are almost completely overlapped. (c) XMCD spectra and integrated XMCD signals from 450 eV at 200 K with a magnetic field $\mu_0 H = 2$ T applied perpendicular to the film surface.

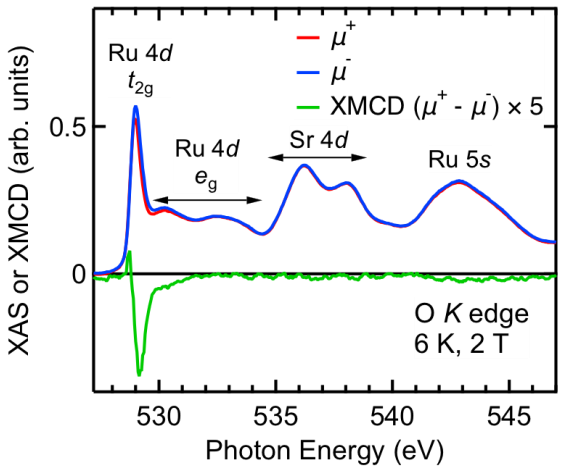

FIG. 6. O *K* edge XAS and XMCD spectra for the $SrRuO_3$ film at 6 K with a magnetic field $\mu_0 H = 2$ T applied perpendicular to the film surface.

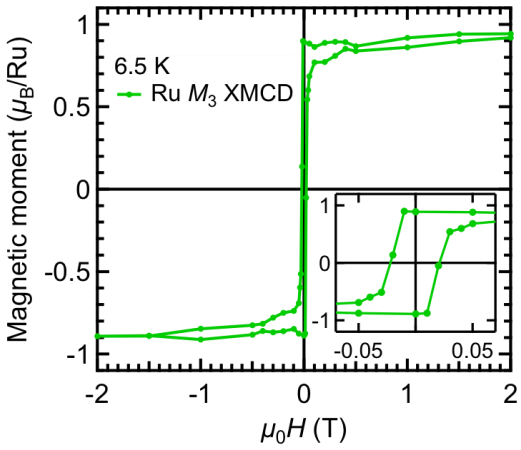

FIG. 7. XMCD-*H* curves measured at the Ru M_3 edge (462.4 eV) for the $SrRuO_3$ film at 6.5 K. The vertical axis of the XMCD intensity at 2 T has been scaled so that it represents the sum of the total magnetic moment $M = m_{\mathrm{spin}} + m_{\mathrm{orb}}$ of the Ru ions estimated from Fig. 4(b).

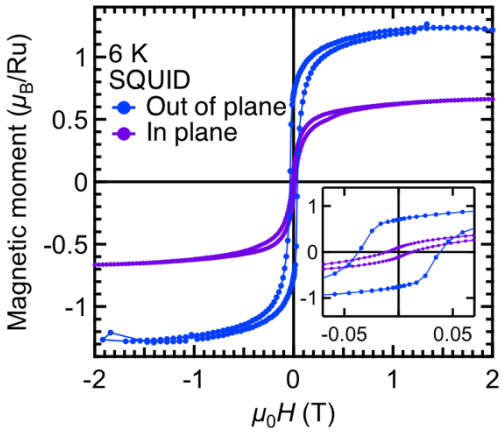

FIG. 8. Magnetic moment vs. H curves for the $SrRuO_3$ film measured by SQUID at 6 K with magnetic fields applied to the out-of-plane [001] (blue circles) and in-plane [100] (purple circles) directions of the $SrTiO_3$ substrate.